



CHORUS

This is the accepted manuscript made available via CHORUS. The article has been published as:

Energy spectrum of thermal counterflow turbulence in superfluid helium-4

J. Gao, E. Varga, W. Guo, and W. F. Vinen

Phys. Rev. B **96**, 094511 — Published 12 September 2017

DOI: [10.1103/PhysRevB.96.094511](https://doi.org/10.1103/PhysRevB.96.094511)

Energy spectrum of Thermal Counterflow Turbulence in Superfluid Helium-4

J. Gao,^{1,2} E. Varga,^{1,3} W. Guo ^{*,1,2} and W.F. Vinen⁴

¹*National High Magnetic Field Laboratory, 1800 East Paul Dirac Drive, Tallahassee, FL 32310, USA*

²*Mechanical Engineering Department, Florida State University, Tallahassee, FL 32310, USA*

³*Faculty of Mathematics and Physics, Charles University, Ke Karlovu 3, 121 16 Prague, Czech Republic*

⁴*School of Physics and Astronomy, University of Birmingham, Birmingham B15 2TT, United Kingdom*

(Dated: August 29, 2017)

Recent preliminary experiments (Marakov *et al* Phys. Rev. **B 91**, 094503 (2015)), using triplet-state He₂ excimer molecules as tracers of the motion of the normal fluid, have shown that, in thermal counterflow turbulence in superfluid ⁴He, small scale turbulence in the superfluid component is accompanied, above a critical heat flux, by partially-coupled large-scale turbulence in both fluids, with an energy spectrum proportional to k^{-m} , where m is greater than the Kolmogorov value of 5/3. Here we report the results of a more detailed study of this spectrum, over a range of temperatures and heat fluxes, using the same experimental technique. We show that the exponent m varies systematically with heat flux, but is always greater than 5/3. We interpret this as arising from the steady counterflow, which causes large-scale eddies in the two fluids to be pulled in opposite directions, giving rise to dissipation by mutual friction at all wave numbers, mutual friction tending also to oppose the effect of the counterflow. Comparison of the experimental results with a simple theory suggests that this process may be more complicated than we might have hoped, but experiments covering a wider range of heat fluxes, which are technically very difficult, will probably be required before we can arrive at a convincing theory.

PACS numbers: 67.25.dk, 29.40.Gx, 47.27.-i

I. INTRODUCTION

Below about 2.17 K, liquid ⁴He undergoes a transition to a superfluid phase (He II) in which an inviscid superfluid component (associated with Bose condensation) coexists with a viscous normal-fluid component (formed from thermal excitations)¹. The flow of the superfluid component must be irrotational. Any rotational motion in a simply-connected volume of superfluid is possible only with the formation of topological defects in the form of quantized vortex lines, each of which carries a circulation of $\kappa = h/m$, where h is Planck's constant and m is the mass of a helium atom². Turbulence in the superfluid component must therefore take the form of a tangle of vortex lines. Turbulence can also occur in the normal fluid, where it is similar to that in a classical fluid, except for the possible presence of a force of mutual friction between the two fluids arising from the scattering of thermal excitations by the vortex lines. Since turbulence in a superfluid is dominated by quantum effects, it is often referred to as quantum turbulence³.

This paper is concerned with the turbulence in a particular form of flow in superfluid helium - the so-called thermal counterflow. When the helium contained in a channel carries a steady heat current, the two fluids are forced to move relative to each other. The normal fluid moves in the direction of the heat current with a mean velocity determined by the heat flux q as $U_n = q/\rho_s T$, where $\rho = \rho_s + \rho_n$ is the total density of the helium, s

is its specific entropy, and T is the temperature. The superfluid moves in the opposite direction with a mean velocity $U_s = (\rho_n/\rho_s)U_n$ to ensure no net mass flow. It was recognized in the 1950s that this forced counterflow can lead to the generation of turbulence in the superfluid component when the counterflow velocity, $U = U_s - U_n$, exceeds a small critical value U_0 ^{4,5}. A phenomenological theory was developed at the same time⁶. A much better understanding was provided by Schwarz⁷, who developed a computer simulation of the counterflow based on the vortex filament model applied to a spatially homogeneous flow. According to this theoretical work, counterflow turbulence exists only in the superfluid component and consists of a more or less random vortex tangle, the velocity field of which exists only on length scales of order, or less than, the average vortex spacing ℓ , which is related to the vortex line density (i.e. length of vortex line per unit volume) L by $\ell = L^{-1/2}$. The dependence of the line density on the counterflow velocity as $L^{1/2} = \gamma U$ was easily understood.

Extensive experimental studies by Tough suggested that this was not the whole story⁸. They showed that there seemed to be two regimes: a TI state characterized by smaller values of γ and a TII state with larger γ . They suggested that transitions to turbulence in the normal fluid might be responsible. Melotte and Barenghi⁹ developed a theory showing that the TI to TII transition might well be associated with an instability in the laminar flow of the normal fluid, leading to a situation in which there is turbulence in both fluids. Experimental confirmation that laminar-to-turbulent transitions do occur in the normal fluid was first provided by Guo *et al*¹⁰, who used metastable He₂^{*} excimer molecules as tracers

*Corresponding: wguo@magnet.fsu.edu

of the motion of the normal fluid. More detailed study of the form of the normal-fluid turbulence was made by Marakov *et al*¹¹ for thermal counterflow in a channel of square cross section with inner side-width $D = 9.5$ mm at a particular temperature of 1.83 K. They showed that the energy spectrum of the normal-fluid turbulence in the heat flux range they studied was of the approximate form $E(k) \propto k^{-2}$ over a range of wave numbers extending from a little larger than $2\pi/D$ to almost $2\pi/\ell$. Over this range of wave numbers the turbulence appeared to be more or less homogeneous. It was argued by Gao *et al*¹², from the observed form of decay of the turbulence when the heat flux is turned off, that this large-scale turbulence in the normal fluid must be coupled through mutual friction to similar large-scale turbulence in the superfluid. The observed energy spectrum describing turbulence on scales much larger than ℓ falls more steeply with increasing wave number than does the Kolmogorov spectrum that describes the inertial sub-range in homogeneous isotropic turbulence in a classical viscous fluid at high Reynolds number. In the absence of the steady counterflow we expect large-scale turbulence in the two fluids to be so strongly coupled by mutual friction that the two velocity fields become almost identical; dissipation is then very small, with the result that there is a single Kolmogorov spectrum³. However, as was discussed by Gao *et al*¹² and in more detail by Babuin *et al*¹³, a steady counterflow will tend to pull turbulent eddies in the two fluids in different directions, causing decoupling, although such decoupling will be opposed by mutual friction. The extent of the decoupling, and hence the magnitude of the resulting dissipation, might then be understood in terms of a balance between two processes: the steady counterflow that is tending to pull the turbulent eddies in the two fluids apart, and mutual friction that is tending to keep them spatially coincident. The theoretical challenge is then to determine whether this process can account for the forms of the observed energy spectra. The extent of the decoupling, and hence the form of the spectrum, can be expected to depend on the eddy size (i.e. the wave number), the strength of the mutual friction, and the counterflow velocity U . Systematic experimental study is therefore called for, from which we can learn how the observed energy spectrum depends on heat flux and temperature. A primary aim of this paper is to report the results of such a study.

Our experimental technique is described in Section II, and the experimental results in Section III. In Section IV, we discuss in a preliminary way whether the observed energy spectra can be understood in terms of a simple balance between the two processes that we have described, and we are led to question whether it can be. Our conclusions are summarised in Section V.

II. COUNTERFLOW EXPERIMENTAL SET-UP

Our experimental setup in this work is similar to the one used in previous studies^{11,12}. As shown in Fig. 1, a stainless steel flow channel with a square cross-section is attached to a pumped helium bath whose temperature can be controlled within 0.1 mK by accurately regulating the vapor pressure. This flow channel has an inner side width of 9.5 mm and a total length of about 300 mm. A planar heater (around 400 Ω) at the lower end of the channel can be used to drive a thermal counterflow. A pair of porous-membrane second sound transducers are installed to excite and detect second-sound standing waves in the channel. The effective area of transducer membrane has a diameter of about 6 mm. The attenuation of the second sound amplitude in the presence of vortex lines allows the determination of the vortex-line density L in the superfluid component^{4,5}.

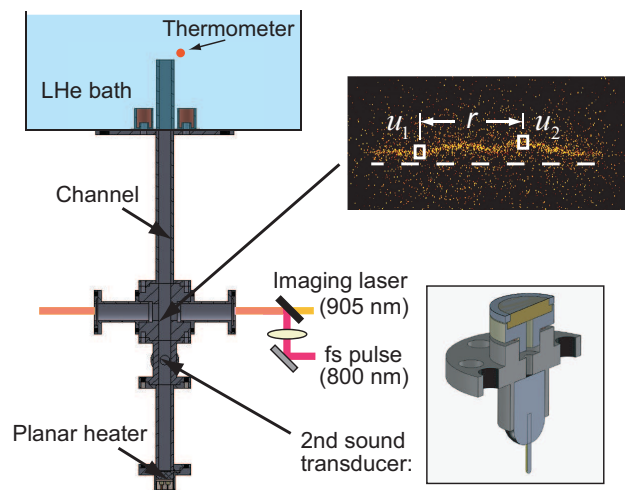


FIG. 1: (color online). Schematic diagram of the experimental setup. A typical image of the He_2^* molecular tracer line in steady-state thermal counterflow is shown. Local stream-wise normal-fluid velocity can be measured, from which the transverse velocity structure function at a given separation r can be determined (see discussions in Section III). The white dashed line indicates the initial location of the tracer line.

In order to probe the normal-fluid motion, we have adopted our recently developed flow visualization technique by tracking thin lines of He_2^* molecular tracers¹⁴. A 35-femtosecond pulsed laser (repetition rate 5 kHz, pulse energy about 60 μJ) is focused into the channel. The beam waist in the focal regime is about 110 μm in diameter. The instantaneous laser intensity in the focal regime is sufficient for ionizing ground state helium atoms to produce a thin line of He_2^* tracer molecules. Above 1 K, these He_2^* tracers are completely entrained by the normal fluid and can be imaged via laser-induced fluorescence from a pulsed imaging laser at 905 nm^{10,15–17}. To pass the laser beams through the channel, two vertical slots (4 mm \times 1.5 mm) are cut into the channel walls. A pair of anti-

reflective coated sapphire windows on two extended side flanges is used to seal the flow. This design helps to avoid laser light scattering in the channel and protect the sapphire windows from high light intensities near the focal region in the centre of the channel. The laser heating in the helium is negligible, as discussed in our previous publication¹⁴. The fluorescence is captured by an intensified CCD (ICCD) camera mounted perpendicularly to both the flow direction and the laser beam path.

In a typical experiment, a straight baseline image is acquired to be used as a reference. Subsequently, we turn on the heater and wait for at least 20 s so that a fully developed counterflow can establish in the channel. Note that due to the relatively large channel width, the temperature gradient across the channel length resulted from typical heat currents used in our experiment is negligible, and hence the thermometer reading should well represent the helium temperature in the channel. We then send in the femtosecond laser pulses to create a tracer line. This tracer line is allowed to move with the normal fluid by a drift time Δt before we send in the imaging laser pulses to produce a fluorescence image. To extract quantitative information, we divide the tracer-line image into many vertical line segments (typically 100 to 200 segments). The line-segment centre position can be determined with a Gaussian fit of its fluorescence intensity profile. The local streamwise velocity of the normal fluid $u_n(R)$ can therefore be computed as the measured line-segment displacement at location R divided by the drift time Δt . In a turbulent flow, a straight tracer deforms randomly due to the turbulent eddy motion. To ensure reliable measurement of the velocity fluctuations resulted from the eddies, we normally use small drift times (typically in the range 10 – 20 ms) so that Δt is shorter than the turnover time of the smallest eddies that can be probed by our visualization method (i.e. $\sim 100 \mu\text{m}$, comparable to the spatial resolution limit).

III. EXPERIMENTAL RESULTS

We have conducted systematic flow visualization and second sound measurements in steady-state counterflow in a range of temperatures and heat fluxes, which greatly extend the parameter range compared to our previous study¹¹. At all temperatures and at sufficiently small heat fluxes, we observe that an initially straight tracer line deforms into a nearly parabolic shape, as we found at 1.83 K¹¹, indicating a laminar Poiseuille normal-fluid velocity profile. As the heat flux is increased towards the turbulence transition, a tail-flattened laminar velocity profile can be observed in the normal fluid, which has recently generated much interest in the quantum turbulence field^{18–20}. At higher heat fluxes, a straight tracer-line deforms randomly, implying turbulent flow in the normal fluid. The turbulent flow regime is the focus in this paper.

At a given temperature and heat flux, we normally

take up to 200 tracer-line images to compute the statistical properties of the turbulent normal-fluid flow. In Fig. 2 (a), the mean normal-fluid velocity $U_n = \langle u_n(R) \rangle$ is shown as a function of the heat flux, where the angle brackets denote ensemble average over all locations across the channel and over all image samples. As one can see, the values of U_n agree well with those calculated from the applied heat flux (i.e. the dashed lines) at all temperatures, confirming that the tracer lines do follow the normal-fluid motion. We have also calculated the streamwise root mean square velocity fluctuation $\Delta u_n = \langle (u_n(R) - U_n)^2 \rangle^{1/2}$. In Fig. 2 (b), we show the turbulence intensity in the normal fluid, defined as $\Delta u_n/U_n$. The observed turbulence intensity is much larger than that in typical classical turbulent channel flows, which is normally a few percent²¹. Note that the turbulence intensity would be smaller if the physically relevant ratio were to involve $U = U_n - U_s$ instead of U_n . The turbulence intensity depends weakly on the heat flux and appears to be controlled solely by the temperature. Fig. 2 (c) shows the temperature dependance of the turbulence intensity averaged over heat fluxes $\overline{\Delta u_n/U_n}$. The mechanism underlying the observed large turbulent intensity in the normal-fluid turbulence is still unclear.

In order to probe the energy spectrum of the normal-fluid turbulence, we have calculated the second-order transverse structure function, defined as $S_2^\perp(r) = \langle [u(R+r/2) - u(R-r/2)]^2 \rangle$, where r is the separation of two line segments as illustrated in Fig. 1. In our calculations, we choose the reference location R at the center of the flow channel. In fact, we observe no significant dependence of the S_2^\perp profile on the reference location. In Fig. 3 (a), typical S_2^\perp curves obtained at various heat fluxes at 1.85 K are shown. Below a few millimeters, our data suggest that $S_2^\perp(r) \propto r^n$, except at the smallest heat flux. The exponent n leads to an energy spectrum $E(k) \sim k^{-(n+1)}$ where k is the wave number^{22,23}. A power law fit to the data (i.e. the dotted lines in Fig. 3 (a)) allows us to determine the exponent n . Note that the heat flux that can be explored in the experiment is limited since the creation of the He_2^* tracer lines is inefficient when the heat flux is too high, as we shall explain later. In our previous report¹¹, $n \simeq 1$ was observed at 1.83 K in the heat flux range 150-300 W/cm². This seemingly different behavior could be caused by the relative large temperature variations in the helium bath in the previous work (i.e., a few mK). There was a level meter in the helium bath which was continuously operated in the previous experiment and hence constantly dissipated heat into the bath). The temperature variations and flows in the bath could affect the counterflow in the channel and result in large uncertainties in the data. This effect is especially significant when the heat current in the channel was small. This level meter was not used during the measurements in our current experiment. In Fig. 3 (b), we show the observed power exponent n at various heat fluxes and temperatures. The uncertainties of the fit in determining n are indicated later in Fig. 6. The black curves in

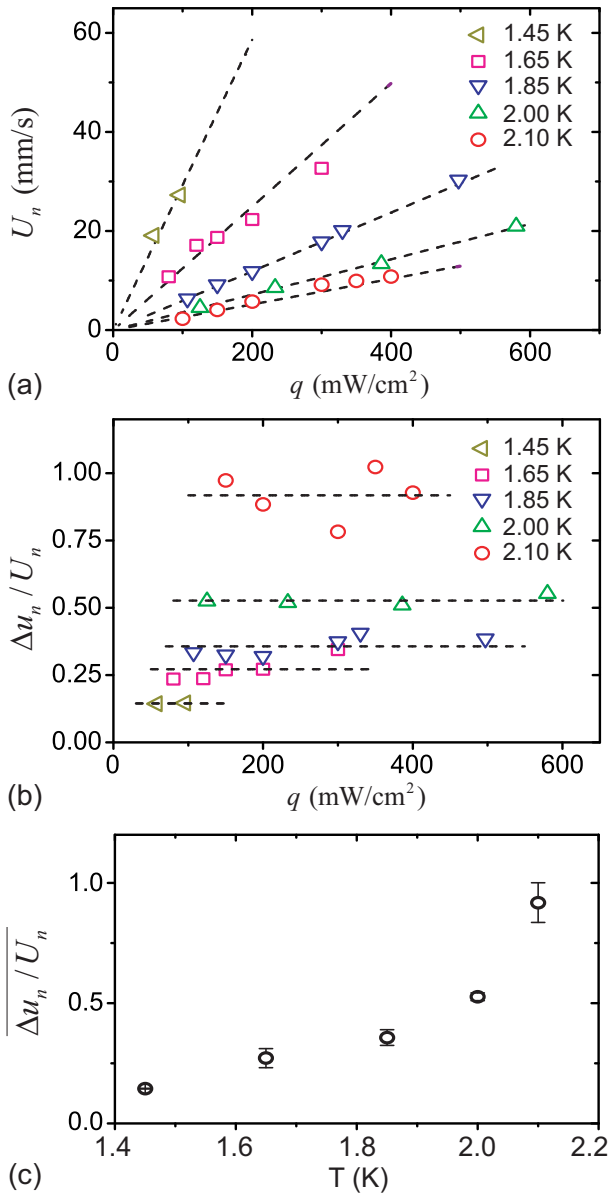


FIG. 2: (color online). (a) Measured mean normal-fluid velocity U_n as a function of heat flux. The dashed lines represent the expected normal-fluid velocity based on two-fluid hydrodynamics¹. (b) Normal-fluid turbulent intensity $\Delta u_n / U_n$ as a function of heat flux at various temperatures. The dashed lines indicate the mean values $\overline{\Delta u_n / U_n}$ averaged over heat fluxes at the different temperatures. (c) Variation of $\overline{\Delta u_n / U_n}$ with temperature.

Fig. 3 (b) represent lines of constant counterflow velocity U . The exponent n appears to vary significantly along these lines, suggesting that the counterflow velocity U is not the controlling factor for the observed spectrum.

In Fig. 4 (a), we show the measured vortex-line density in steady counterflow using the standard second sound attenuation method^{4,5}. As we have already noted, it is expected that $L^{1/2} = \gamma(U - U_0)$. A linear dependence of $L^{1/2}$ on U is indeed seen at all temperatures. We per-

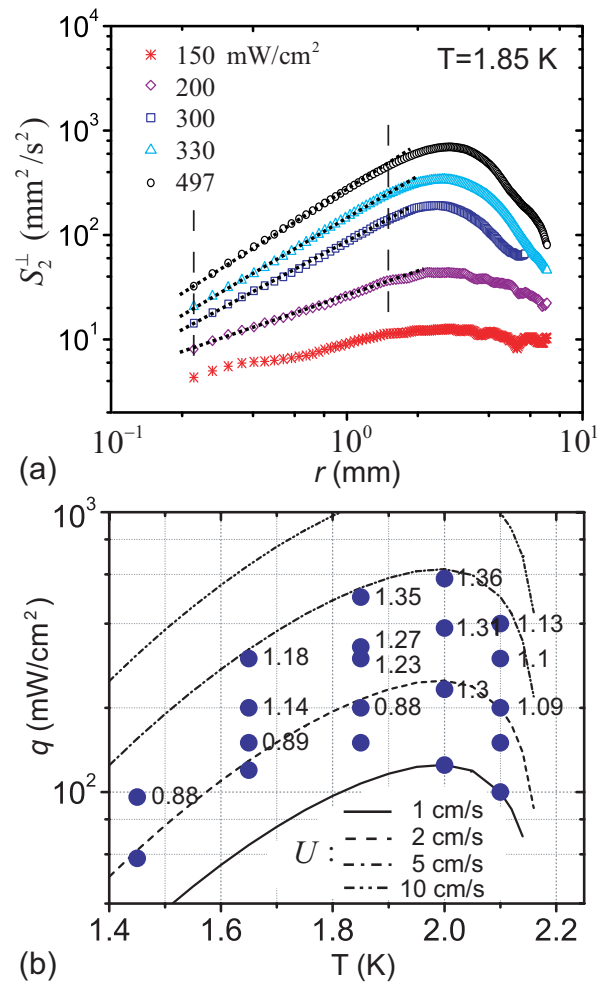


FIG. 3: (color online). (a) Typical calculated second order transverse structure function $S_2^\perp(r)$ at various heat fluxes. The data shown were obtained at 1.85 K. The dotted lines represent the power-law r^n fit to the data. The vertical dashed lines indicated the range of the power-law fit. At the lowest heat flux, the $S_2^\perp(r)$ curve does not show clear power-law regime. (b) The observed power exponent n at various heat fluxes and temperatures. The n values at low heat fluxes are skipped since the power-law fit appears no longer reliable.

form a linear fit to the data to determine the γ coefficient and the critical velocity U_0 . The resulting values of γ as a function of temperature are shown in Fig. 4 (b). For comparison, we have also included the γ values in counterflow reported by other groups²⁴⁻²⁹. The data points scatter among experiments, which may be caused by the different sizes of the channels used in different experiments. The overall trend of our data appear to agree better with those reported in the TII state. This is perhaps not surprising since, in the heat flux range we used, the flows in both the superfluid and the normal-fluid components are turbulent on a large scale. The critical velocity U_0 we have obtained is around 2 mm/s with no obvious dependence on temperature, in agreement with early studies^{29,30}.

TABLE I: The flow visualization and second sound measurement results at selected temperatures and heat fluxes.

T (K)	q (mW/cm ²)	U_n (mm/s)	Δu_n (mm/s)	$\overline{\Delta u_n/U_n}$	n	L (cm ⁻²)	γ (s/cm ²)	$Z(k_0)$
1.65	150	18.7	5.0	0.272	0.89±0.03	8.63×10^4	139.9±2.4	1.44
	200	22.3	6.1		1.14±0.03	1.62×10^5		1.02
	300	32.7	11.2		1.18±0.04	3.82×10^5 ^a		0.65
1.85	200	11.8	3.8	0.357	0.88±0.04	8.11×10^4	173.6±5.8	1.41
	300	17.8	6.7		1.23±0.02	1.98×10^5		0.87
	330	20.1	8.1		1.27±0.03	2.48×10^5		0.76
	497	30.3	11.7		1.35±0.03	5.85×10^5 ^a		0.48
2.0	233	8.6	4.4	0.526	1.3±0.02	1.41×10^5	242.8±12.1	0.80
	386	13.4	6.8		1.31±0.03	4.73×10^5		0.39
	580	20.9	11.6		1.36±0.02	1.12×10^6 ^a		0.25
2.1	200	5.7	5.1	0.918	1.09±0.02	3.73×10^5	303.6	0.24
	350	9.92	10.1		1.11±0.04	1.14×10^6 ^a		0.14

^aValues are extrapolated from Fig. 4 (a).

In order to aid the discussions in Section IV, we list some measured results in Table I at temperatures and heat fluxes where both the second sound data and visualization data are available.

IV. DISCUSSION

In discussing our experimentally observed structure functions, and the energy spectra that can be deduced from them, we shall make the following assumptions. (1) Turbulent energy is injected on two length scales: one, on a scale of order the vortex line spacing, enters the superfluid only, by the mechanism identified by Schwarz⁷; the other, on a scale comparable with the width, D , of the channel, enters initially either the superfluid component or the normal component or both, although if it enters only one component it may be transferred quickly to the other by mutual friction, as we shall explain. (2) The turbulent energy injected on the large scale is transferred by non-linear effects through a form of Richardson cascade to smaller scales, this cascade being characterised by the energy spectra that we have observed. (3) The steady counterflow velocities, U_s and U_n , are spatially uniform. Although these assumptions form a reasonable starting point for our discussion, they are not necessarily correct; for example, energy injection might conceivably occur also on other, intermediate, length scales.

In the absence of a counterflow, mutual friction would quickly lead to essentially complete coupling of the large scale turbulence in each fluid, the turbulent velocities u_s and u_n becoming essentially equal³. There would then be no dissipation in the cascade on scales larger than ℓ , and in the associated inertial sub-range there would be an energy spectrum that is, approximately, of the Kolmogorov form $E(k) = C\epsilon^{2/3}k^{-5/3}$. However, as we have mentioned, the steady counterflow will tend to pull the turbulent eddies in the two fluids in opposite directions (the effect of the terms $(U_s \cdot \nabla)u_s$ and $(U_n \cdot \nabla)u_n$ in

the equations of motion). This decoupling effect is opposed by mutual friction to an extent that depends, for motion on a scale $2\pi/k$, on the dimensionless parameter $Z(k) = kU\tau$, where $U = U_s - U_n$ and $\tau = \rho_n/\rho_s\alpha\kappa L$ (α is the dimensionless mutual friction parameter); the relevance of this parameter has already been discussed by Babuin *et al*¹³. The characteristic time τ determines³ the rate at which mutual friction tends to eliminate the velocity difference $(u_s - u_n)$, while $(kU)^{-1}$ is the time taken by the counterflow to decouple eddies of size $2\pi/k$. Any decoupling on a scale $2\pi/k$ will lead to dissipation on this scale and hence to a departure from the Kolmogorov spectrum. On the basis of very simple assumptions, we shall now estimate the magnitudes of these departures for different values of Z .

Let us first consider the case $Z(k) \gg 1$, when decoupling can be expected to be complete for all relevant k . The turbulent velocity fluctuations in the normal fluid, u_n , are then assumed to be uncorrelated with those in the superfluid, so that the turbulent motion in the normal fluid can be assumed to be damped as though the superfluid were constrained to be at rest. The damping is characterised by a time constant $\tau_1 = \rho_n/\rho_s\alpha\kappa L$. We need to understand how this damping affects the energy spectrum in the normal fluid. We note that a similar problem arises in the development of a theory of homogeneous isotropic turbulence in superfluid ³He-B. In this case the normal fluid has such a large viscosity that it cannot become turbulent, so that turbulence in the superfluid component evolves in the presence of a normal fluid that is constrained to be at rest. There is an obvious similarity between this situation and that for $Z(k) \gg 1$ in our case, except that the roles of the two fluids are reversed (this similarity has already been noted by Babuin *et al*¹³). The ³He problem has been addressed in the literature in various ways; one of us based our discussion³¹ on an appropriate solution of a modified ‘‘Leith’’ differential equation³² that describes the diffusion of turbulent energy in k -space, while reference to other approaches

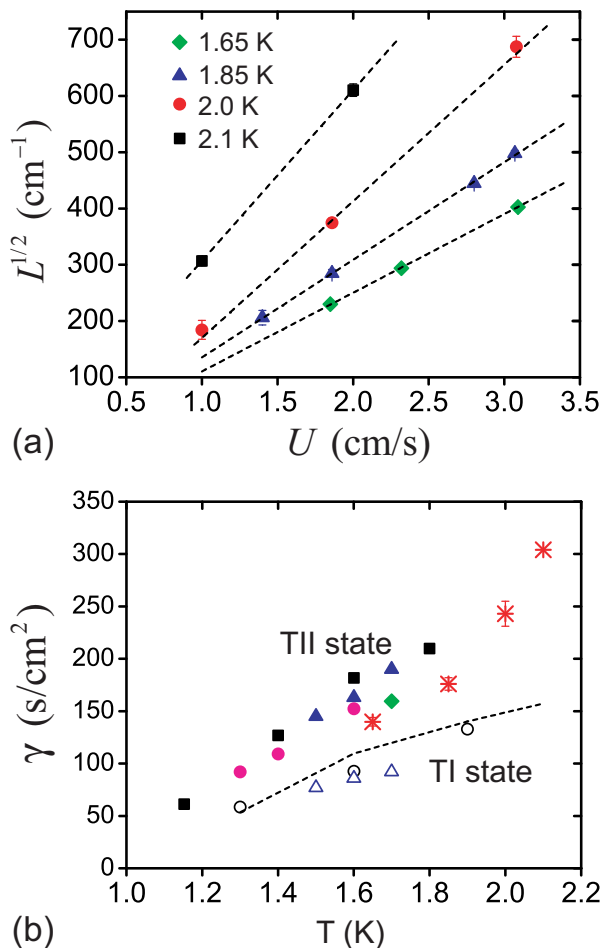


FIG. 4: (color online). (a) Square root of the measured vortex-line density $L^{1/2}$ as a function of the mean counterflow velocity U . The dashed lines represent linear fits to the data. (b) The derived γ coefficients in thermal counterflow as a function of temperature. The red asterisks, this work; the solid black squares, by Chase, 0.8-mm diameter circular channel²⁴; the solid magenta circles, by Dimotakis and Broadwell, 3.18-mm diameter circular channel²⁵; the solid blue triangles (TII state) and the open blue triangles (TI state), by Martin and Tough, 1-mm diameter circular channel²⁷; the green diamond, by Babuin *et al.*, 7-mm side width square channel²⁹; the open black circles (TI state), by Childers and Tough, 0.13-mm diameter circular channel²⁶; the dashed line, by Adachi *et al.*, numerical simulation for TI state²⁸.

is included in ref [13]. Here we shall adopt a different, simpler, and perhaps more transparent approach, which will serve adequately to provide us with the answers we require.

We write the energy spectrum in the form

$$E(k) = [\epsilon(k)]^{2/3} k^{-5/3}, \quad (1)$$

recognizing that the dissipation must lead to an energy flux ϵ that decreases with increasing wave number. Tentatively, we shall assume that the spectrum takes the

form

$$E(k) = Ak^{-p}(1 + Bk^q), \quad (2)$$

where A , p and q prove to be constants that we must determine and B to be an adjustable parameter.

We note that $kE(k)$ can be assumed to be the energy associated with eddies of size $2\pi/k$, and that $k d\epsilon/dk$ can be assumed to be the rate of energy dissipation in these eddies. It follows that

$$k \frac{d\epsilon}{dk} = -\frac{2kE(k)}{\tau_1} = -\frac{2Ak^{1-p}}{\tau_1}(1 + Bk^q). \quad (3)$$

Integration then leads to

$$\epsilon = -\frac{2Ak^{1-p}}{(1-p)\tau_1} \left(1 + \frac{B(1-p)}{q-p+1} k^q\right). \quad (4)$$

Let us now assume that $Bk^q \ll 1$. Then, approximately,

$$E(k) = \left(\frac{2A}{(p-1)\tau_1}\right)^{2/3} \left(1 + \frac{2B(1-p)}{3(q-p+1)} k^q\right) k^{-(1+2p/3)}. \quad (5)$$

Comparing this equation with Eq.(2), we see that $p = 3$, $A = \tau_1^{-2}$ and $q = 4/3$. Therefore

$$E(k) = \frac{1}{\tau_1^2} k^{-3}(1 + Bk^{4/3}), \quad (6)$$

if $Bk^{4/3} \ll 1$.

The behaviour of $E(k)$ is quite different according as B is greater than or less than zero. Consider the behaviour of the product $k^{5/3}E(k)$, which has a constant value for a Kolmogorov spectrum. According to Eq.(6) this product behaves as shown schematically in Fig.5. Of course, Eq.(6) is not strictly valid when $Bk^{4/3}$ is not small, but the behaviour shown in Fig.5 remains qualitatively correct. In fact, we expect the spectrum $E(k)$ to tend towards the Kolmogorov form when dissipation starts to become unimportant: i.e. when τ_1 becomes much larger than the eddy turnover time $2\pi/ku_n(k)$ (where $u_n(k)$ is the turbulent velocity in the normal fluid on a scale $2\pi/k$), a condition that can be written as

$$ku_n(k)\tau_1 \gg 2\pi. \quad (7)$$

This condition can be satisfied only if $B > 0$. If $B < 0$, the product $k^{5/3}E(k)$ falls more and more steeply as k increases, until it vanishes at a finite k , as shown schematically in Fig.5.

Which of these two scenarios applies depends on the rate of injection of energy at the injection wave number k_0 , a rate that is equal to $k_0[u_n(k_0)]^3/4\pi$. As we see from Eq.(4), if this rate of injection exceeds $(k_0^2\tau_1^3)^{-2}$ (i.e. if $k_0u_0(k_0)\tau_1 > (4\pi)^{1/3}$) then $B > 1$, and $E(k)$ must tend towards Kolmogorov at sufficiently large k . Otherwise $E(k)$ falls to zero at a finite k , and $E(k)$ always falls more steeply than k^{-3} . In practice, $u_n(k_0)$ is, for a given temperature, a fixed fraction of U : $u_n(k_0) = \chi U$ (we

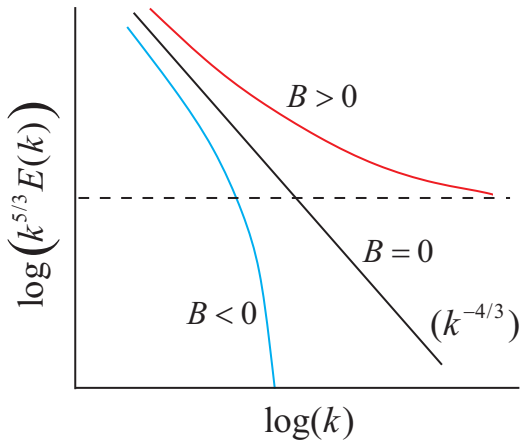


FIG. 5: (color online). Schematic diagram showing the theoretical energy spectrum for different values of B .

can take $u_n(k_0) = \Delta u_n$ to a reasonable approximation, since most of the turbulent energy is at small wave numbers). Therefore the condition that $E(k)$ tends towards Kolmogorov at sufficiently large k can be written as

$$Z(k_0) > \frac{\rho_s}{\rho\chi} (4\pi)^{1/3}. \quad (8)$$

However, $E(k)$ will have the actual Kolmogorov form for all $k > k_0$ only if the following more stringent condition is satisfied

$$Z(k_0) \gg \frac{\rho_s}{\rho\chi} (2\pi), \quad (9)$$

as we see from Eq.(7); otherwise, $E(k)$ will fall with increasing k as roughly k^{-3} . Values of the right hand sides of the inequalities (8) and (9) are given in Table II. We remark here that in interpreting our experiments we shall take k_0 to be equal to $2\pi/(2\text{mm})$, since the observed structure functions have maximum values at $r \approx 2\text{mm}$; our observed energy spectra then relate to the range of k from k_0 to about $10k_0$.

TABLE II: Values of various parameters at different temperatures.

$T(\text{K})$	χ	$\frac{\rho_s}{\rho\chi} (4\pi)^{1/3}$	$\frac{\rho_s}{\rho\chi} (2\pi)$	$\left(\frac{\rho\chi}{\rho_s}\right)^{3/4}$
1.65	0.22	8.53	23.1	0.38
1.85	0.23	6.51	17.6	0.47
2.0	0.22	4.42	11.9	0.59
2.1	0.24	2.53	6.85	0.94

We turn now to the condition when there is strong coupling: $Z(k) \ll 1$. The normal and superfluid eddies are then forced into approximate coincidence, so that $(u_n - u_s) \ll u_n$. It is easily shown from the two-fluid equations of motion that the small decoupling is

described approximately by the equation

$$(U \cdot \nabla) u_n = \frac{1}{\tau} (u_s - u_n), \quad (10)$$

so that the small average value of $(u_s - u_n)$ for wave number k can be estimated as being given by

$$\langle |u_s - u_n| \rangle \sim \tau U \left\langle \left| \frac{\partial u_n}{\partial x} \right| \right\rangle \sim k U \tau u_n = Z(k) u_n, \quad (11)$$

for eddies centred on wave number k . It follows that the corresponding dissipation per unit volume of helium is given by

$$W \sim \frac{\langle |u_s - u_n|^2 \rangle}{\tau} = Z(k)^2 \frac{u_n^2}{\tau}, \quad (12)$$

where we have assumed that the sign of $(u_s - u_n)$ is random. However, as can be shown fairly easily, only a fraction ρ_s/ρ of this dissipation is associated with the normal fluid. We see that the dissipation in the normal fluid is proportional to k^2 , so that its effect on the energy spectrum is similar to that of viscosity. Since the dissipation due to a kinematic viscosity ν is $\nu k^2 u_n^2$, the effective kinematic viscosity is given roughly by

$$\nu_{\text{eff}} = \frac{\rho_s}{\rho} U^2 \tau = \frac{\rho_s U}{\rho k_0} Z(k_0). \quad (13)$$

This effective kinematic viscosity has a typical value of $3 \times 10^{-6} \text{m}^2 \text{s}^{-1}$. It will therefore have little effect on the Kolmogorov energy spectrum at sufficiently small wave numbers, but it will lead to a cut-off when the wave number exceeds the critical value given by

$$k_c = \left(\frac{\epsilon}{\nu_{\text{eff}}^3} \right)^{1/4}, \quad (14)$$

where ϵ is the energy flux down the inertial part of the Richardson cascade. Taking $\epsilon = k_0 [u_n(k_0)]^3 / 4\pi$, we find that

$$\frac{k_c}{k_0} = \frac{1}{(4\pi)^{1/4} Z(k_0)} \left(\frac{\rho\chi}{\rho_s} \right)^{3/4}. \quad (15)$$

As we have mentioned, our experiments relate to the energy spectrum over a range of wave numbers from k_0 to $10k_0$. Thus we can expect to see a Kolmogorov energy spectrum only if

$$Z(k_0) \ll 0.05 \left(\frac{\rho\chi}{\rho_s} \right)^{3/4}. \quad (16)$$

Otherwise the spectrum ought to fall more steeply with increasing k than is the case for a Kolmogorov spectrum. Values of the parameter $(\rho\chi/\rho_s)^{3/4}$ at different temperatures are included in Table II. We note that $k_c \sim k_0$ when $Z(k_0) \sim 0.25$.

We note that our discussion leads to the conclusion that, over limited ranges of k , the energy spectrum

should be of the form $E(k) \propto k^{-m}$, where, for a given temperature, the exponent m is a function of $Z(k_0)$. Therefore in Fig.6 we have plotted our experimental results for $m = n + 1$ against $Z(k_0)$. Remember that we have taken $2\pi/k_0 = 2$ mm, since the maximum in the second-order structure function is situated at $r = 2$ mm.

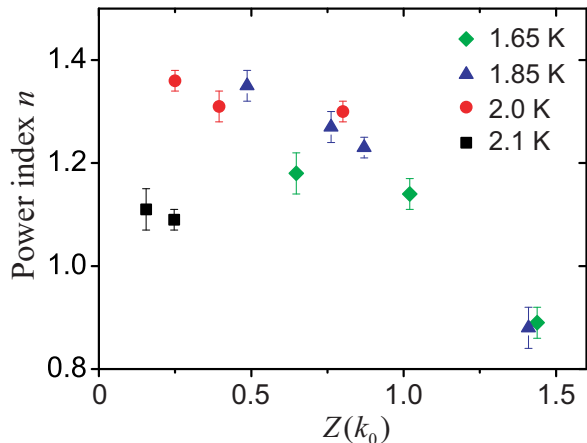


FIG. 6: (color online). The power exponent n of the second order transverse structure function S_2^\perp as a function of $Z(k_0)$, with $k_0 = 2\pi/2$ mm.

The arguments that we have summarised so far serve to establish how the counterflow energy spectrum for large-scale turbulence in the normal fluid is likely to behave in various limits, according to our simple de-coupling theory. Unfortunately, our experimental results do not relate strictly to any of these limits; they cover only a small range of values of $Z(k_0)$ of order unity. Nevertheless we can examine our results to see whether they might, or might not, be consistent with our theoretical predictions.

In all cases we observe an energy spectrum $E(k) \propto k^{-m}$ (remember that $m = n+1$). Let us make the reasonable assumption that for a given temperature our simple de-coupling theory would lead to a smooth variation of m with $Z(k_0)$. Based on our analysis of the asymptotic forms of behaviour we would then expect m to vary with $Z(k_0)$ in the way sketched roughly and schematically in Fig.7.

We note that experiment suggests, but does not yet firmly establish, that the value of m , as a function of $Z(k_0)$, passes through a maximum at around $Z(k_0) = 0.5$, in qualitative agreement with theory. However, quantitatively, experiment differs from our tentative theory in two respects: the magnitude of m in the region of the maximum (if it exists) is smaller; and, probably more seriously, m seems to be falling rapidly to the Kolmogorov value at $Z(k_0) \sim 1.5$, rather than at $Z(k_0) \sim 20$, as suggested by the theory. The latter difference seems to us more serious, because it is hard to see, on the basis of our assumptions, how the energy spectrum can be close to Kolmogorov when $Z(k_0) \sim 1$. Therefore we draw the tentative conclusion that the theory is inadequate, most obviously if $Z(k_0) > 1$, because the assumptions on

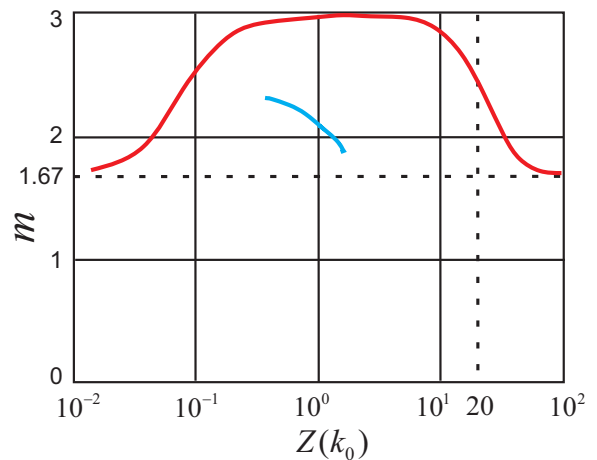


FIG. 7: (color online). Sketches of the power exponent m of the energy spectrum as a function of $Z(k_0)$. Red line: suggested theory (1.85 K); Blue line: experiment (1.85 K).

which it is based are wrong. This in turn suggests that, contrary to our supposition, the condition $Z(k_0) \gg 1$ does not signal a complete breakdown of coupling between large scale turbulence in the two fluids. We are presently working on the formulation of a version of the Leith equation that will allow us to predict the energy spectra for any value of $Z(k_0)$. Tentative results are consistent with the conclusions that we have just drawn, and do not serve to give better agreement with experiment. One possibility is that mutual friction is serving not only to damp the turbulent motion in each fluid, but also to generate extra turbulence, as occurs, for special reasons identified by Schwarz⁷, on scales of order the vortex line spacing. The development of an improved theory may be seriously challenging.

In the light of our discussion it is very clear that our measurements cover a range of values of $Z(k_0)$ that is far too small. The range of $Z(k_0)$ is determined largely by the range of heat fluxes that can be studied. Small values of $Z(k_0)$ correspond to large heat fluxes, and *vice versa*. In our experiments the smallest accessible heat fluxes are determined by the critical velocity below which there is no large-scale turbulence. The largest accessible heat fluxes are determined by a technical limitation arising from the way in which a sufficiently dense initial line of excimer molecules is generated. For reasons that are explained in ref [14], an adequate density can be achieved only if several pulses of the femtosecond laser are used, later pulses relying on the ionization of excimer molecules produced by earlier pulses. It follows that the heat flux cannot be too large: otherwise the motion of the normal fluid will sweep the excimer molecules produced by earlier pulses away from the beam line of the later pulses. Overcoming this limitation is a challenge for the future.

V. CONCLUSION

When superfluid ^4He carries a heat current, with a resulting counterflow of the two fluids, turbulence is generated in the superfluid component on a length scale comparable with the vortex line spacing, as has been known and understood for many years. Recently it has been discovered that, above a certain critical heat flux, this small scale turbulence is accompanied by turbulence in both fluids on scales up to the size of the containing channel. We have reported a new experimental study of the large-scale turbulence in the normal fluid, based on the use of metastable triplet-state He_2 excimer molecules as tracers. This study has yielded information about the energy spectrum characterising this turbulence, over a range of temperatures and heat fluxes. The spectrum has usually the form $E(k) \propto k^{-m}$, where m varies with temperature and heat flux and is always greater than the Kolmogorov value of $5/3$; this value applies to the inertial sub-range in homogeneous isotropic turbulence in a classical fluid, and also in superfluid ^4He when turbulent flow of the two fluids can be fully coupled by mutual friction. The increased value of m is attributed to dissipation arising from a breakdown in this coupling caused by the steady counterflow. A simple theory of this decoupling is shown to lead to results that may be in qualitative agreement with experiment, but are not in quantitative agreement.

The simple assumptions underlying this theory are therefore probably wrong.

Acknowledgments

Some of the ideas developed in Section IV appear also in ref [13]. The two groups concerned have been working in parallel and independently for some years, often generating ideas that are very similar in the underlying physics, a fact that has been acknowledged in one joint publication¹². However, the precise way in which these ideas have been developed is usually very different. We offer our own approach here, while drawing attention to, and acknowledging, the approach in ref [13]. Our view that some of the ideas in Section IV are actually in conflict with experiment is, we believe, new.

J.G. and W.G. acknowledge the support from the US Department of Energy under Grant No. DE-FG02 96ER40952 and the National Science Foundation under Grant No. DMR-1507386. The work was conducted at the National High Magnetic Field Laboratory, which is supported by NSF DMR-1157490 and the State of Florida. The authors would also like to thank D. N. McKinsey and S. W. Van Sciver for providing laser and cryogenics equipment.

-
- ¹ D.R. Tilley and J. Tilley, *Superfluidity and Superconductivity* (2nd Ed, Adam Hilger, Bristol, 1986).
- ² R.J. Donnelly, *Quantized Vortices in Helium II*, (Cambridge University Press, Cambridge, England, 1991).
- ³ W.F. Vinen and J.J. Niemela, *J. Low Temp. Phys.*, **126**, 167-231 (2002).
- ⁴ W. F. Vinen, *Proc. R. Soc.* **240**, 114 (1957).
- ⁵ W. F. Vinen, *Proc. R. Soc.* **240**, 128 (1957).
- ⁶ W. F. Vinen, *Proc. R. Soc.* **242**, 493 (1957).
- ⁷ K. W. Schwarz, *Phys. Rev.* **B 38**, 2398 (1988).
- ⁸ J. T. Tough, *Superfluid turbulence*, in *Progress in Low Temperature Physics*, Vol. VIII (North-Holland, Amsterdam, 1982).
- ⁹ D. J. Melotte and C. F. Barenghi, *Phys. Rev. Lett.* **80**, 4181 (1998).
- ¹⁰ W. Guo, S. B. Cahn, J. A. Nikkel, W. F. Vinen, and D. N. McKinsey, *Phys. Rev. Lett.* **105**, 045301 (2010).
- ¹¹ A. Marakov, J. Gao, W. Guo, S. W. Van Sciver, G. G. Ihas, D. N. McKinsey, and W. F. Vinen, *Phys. Rev.* **B 91**, 094503 (2015).
- ¹² J. Gao, W. Guo, V.S. L'Vov, A. Pomyalov, L. Skrbek, E. Varga, and W.F. Vinen, *JETP Letters*, 103, 732 (2016).
- ¹³ S. Babuin, V. S. L'vov, A. Pomyalov, L. Skrbek, and E. Varga, *Phys. Rev.* **B 94**, 174504 (2016).
- ¹⁴ J. Gao, A. Marakov, W. Guo, B.T. Pawlowski, S.W. Van Sciver, G.G. Ihas, D.N. McKinsey, and W.F. Vinen, *Rev. Sci. Instrum.*, **86**, 093904 (2015).
- ¹⁵ W.G. Rellergert, S.B. Cahn, A. Garvan, J.C. Hanson, W.H. Lippincott, J.A. Nikkel, and D.N. McKinsey, *Phys. Rev. Lett.*, **100**, 025301 (2008).
- ¹⁶ W. Guo, J.D. Wright, S.B. Cahn, J.A. Nikkel, and D.N. McKinsey, *Phys. Rev. Lett.*, **102**, 235301/1-4 (2009).
- ¹⁷ W. Guo, M. La Mantia, D.P. Lathrop, and S.W. Van Sciver, *Proc. Natl. Acad. Sci.*, **111**, 4653 (2014).
- ¹⁸ S. Yui and M. Tsubota, *Phys. Rev.* **B 91**, 184504 (2015).
- ¹⁹ L. Galantucci, M. Sciacca, and C.F. Barenghi, *Phys. Rev.* **B 92**, 174530 (2015).
- ²⁰ D. Khomenko, P. Mishra, and A. Pomyalov, *J. Low Temp. Phys.*, **187**, 405 (2017).
- ²¹ P.A. Davidson, *Turbulence: An Introduction for Scientists and Engineers* (Oxford University Press, UK, 2004).
- ²² A.N. Kolmogorov, *C. R. Acad. Sci. USSR*, **32**, 16-18 (1941).
- ²³ U. Frisch, *Turbulence: The Legacy of A. N. Kolmogorov* (Cambridge Univ. Press, Cambridge, MA, U.S.A., 1995).
- ²⁴ C. E. Chase, *Phys. Rev.* **127**, 361 (1962).
- ²⁵ P. E. Dimotakis and J. E. Broadwell, *Phys. Fluids*, **16**, 1787 (1973).
- ²⁶ R. K. Childers and J. T. Tough, *Phys. Rev.* **B 13**, 1040 (1976).
- ²⁷ K. P. Martin and J. T. Tough, *Phys. Rev.* **B 27**, 2788 (1983).
- ²⁸ H. Adachi, S. Fujiyama, and M. Tsubota, *Phys. Rev.* **B 81**, 104511 (2010).
- ²⁹ S. Babuin, M. Stammeier, E. Varga, M. Rotter, and L. Skrbek, *Phys. Rev.* **B 86**, 134515 (2012).
- ³⁰ E. Varga, S. Babuin, and L. Skrbek, *Phys. Fluids* **27**, 065101 (2015).
- ³¹ W. F. Vinen, *Phys. Rev.* **B 71**, 024513 (2005).
- ³² C. E. Leith, *Phys. Fluids* **10**, 1409 (1967).